

# Heavy sfermions in SUSY analysis at LHC and ILC

K. Desch<sup>1</sup>, J. Kalinowski<sup>2</sup>, G. Moortgat-Pick<sup>3a</sup>, K. Rolbiecki<sup>2</sup>, and W.J. Stirling<sup>3</sup>

<sup>1</sup> Physikalisches Institut, Universität Bonn, D-53115 Bonn, Germany

<sup>2</sup> Instytut Fizyki Teoretycznej, Uniwersytet Warszawski, PL-00681, Warsaw, Poland

<sup>3</sup> IPPP, Institute of Particle Physics Phenomenology, University of Durham, Durham DH1 3LE, UK

**Abstract.** The physics potential of the Large Hadron Collider in combination with the planned International Linear Collider is discussed for a difficult region of supersymmetry that is characterized by scalar SUSY particles with masses around 2 TeV. Precision measurements of masses, cross sections and forward-backward asymmetries allow to determine the fundamental supersymmetric parameters even if only a small part of the spectrum is accessible. No assumptions on a specific SUSY-breaking mechanism are imposed. Mass constraints for the kinematically inaccessible particles can be derived.

**PACS.** 14.80.Ly Supersymmetric partners of known particles – 11.30.Pb Supersymmetry

## 1 Introduction

Supersymmetry (SUSY) is one of the best-motivated candidates for physics beyond the Standard Model (SM). If experiments at future accelerators, the Large Hadron Collider (LHC) and the International Linear Collider (ILC), discover SUSY they will have as well to determine precisely the underlying SUSY-breaking scenario with as few theoretical prejudices as possible. Scenarios where the scalar SUSY particle sector is very heavy as required, for instance, in focus-point scenarios (FP) [1] are particularly challenging. In these scenarios the gaugino masses are kept relatively small while squark and slepton masses might be in the multi-TeV range. It is therefore of particular interest to verify whether the interplay of a combined LHC/ILC analysis [2] could unravel such models with very heavy sfermions.

Methods to derive the SUSY parameters at collider experiments have been worked out, for instance in [3,4]. In [5,6,7] the chargino and neutralino sectors have been exploited at the ILC to determine the MSSM parameters. However, in most cases only the production processes have been studied. Furthermore, it has been assumed that the masses of the virtual scalar particles are already known. In the case of heavy scalars such assumptions, however, cannot be applied and further observables have to be used to determine the underlying parameters. Studies have been made to exploit the whole production-and-decay process in the chargino/neutralino sector [8]. Exploiting spin effects, it has been shown in [9] that, once the chargino parameters are known, useful indirect bounds for the mass of the heavy virtual particles could be derived

from forward-backward asymmetries of the final lepton  $A_{\text{FB}}(\ell)$ .

Here a FP-inspired scenario is discussed that is characterized by a  $\sim 2$  TeV scalar particles sector [10]. In addition, the neutralino sector turns out to have very low production cross sections in  $e^+e^-$  collisions, so that it might not be fully exploitable. Only the chargino pair production process has high rates and all information obtainable from this sector has to be used. The analysis is performed entirely at the EW scale, without any reference to the underlying SUSY-breaking mechanism. Masses, cross sections and spin-dependent forward-backward asymmetries are measured at the LHC and at the ILC with  $\sqrt{s} \leq 500$  GeV. The potential of a multiparameter fit to determine the underlying parameters has been analysed.

## 2 Case study at LHC and ILC

We study chargino production with subsequent leptonic and hadronic decays

$$e^- + e^+ \rightarrow \tilde{\chi}_1^+ + \tilde{\chi}_1^-, \quad (1)$$

$$\tilde{\chi}_1^+ \rightarrow \tilde{\chi}_1^0 + \ell^+ + \nu \quad \text{and} \quad \tilde{\chi}_1^0 + \bar{q}_d + q_u, \quad (2)$$

$$\tilde{\chi}_1^- \rightarrow \tilde{\chi}_1^0 + \ell^- + \bar{\nu} \quad \text{and} \quad \tilde{\chi}_1^0 + q_d + \bar{q}_u, \quad (3)$$

where  $\ell = e, \mu$ ,  $q_u = u, c$ ,  $q_d = d, s$ . The production process contains contributions from  $\gamma$ - and  $Z^0$ -exchange in the  $s$ -channel and from  $\tilde{\nu}$ -exchange in the  $t$ -channel. The decay processes are mediated by  $W^\pm$ ,  $\tilde{\ell}_L$ ,  $\tilde{\nu}$  or by  $\tilde{q}_{dL}$ ,  $\tilde{q}_{uL}$  exchange. The masses and eigenstates of the neutralinos and charginos are determined by the fundamental SUSY parameters: the  $U(1)$ ,  $SU(2)$  gaugino mass parameters  $M_1$ ,  $M_2$ , the Higgs mass parameter  $\mu$  and the ratio of the vacuum expectation values of the two neutral Higgs fields,  $\tan \beta = \frac{v_2}{v_1}$ .

<sup>a</sup> Email: g.a.moortgat-pick@durham.ac.uk

The chosen MSSM scenario can be characterized via the following mSUGRA parameters, taken at the GUT scale except for  $\tan\beta$ :  $m_{1/2} = 144$  GeV,  $m_0 = 2$  TeV,  $A_0 = 0$  GeV,  $\tan\beta = 20$ ,  $\text{sgn}(\mu) = +1$ . However, our analysis is performed completely within the general MSSM framework, without any reference to the underlying SUSY-breaking mechanism. The parameters at the EW scale are given by

$$\begin{aligned} M_1 &= 60 \text{ GeV}, & M_2 &= 121 \text{ GeV}, & M_3 &= 322 \text{ GeV} \\ \mu &= 540 \text{ GeV}, & \tan\beta &= 20 \end{aligned} \quad (4)$$

The derived masses of the SUSY particles are listed in Table 1. As can be seen, the charginos and neutralinos as well as the gluino are rather light, whereas the scalar SUSY particles have masses about 2 TeV.

## 2.1 Expectations at the LHC

All squarks in this scenario are kinematically accessible at the LHC. The largest squark production cross section is for  $\tilde{t}_{1,2}$ . However, with stops decaying mainly to  $\tilde{g}t$  (with  $BR(\tilde{t}_{1,2} \rightarrow \tilde{g}t) \sim 66\%$ ), where background from top production will be large, no new interesting channels are open in their decays. The other squarks decay mainly via  $\tilde{g}q$ , but since the squarks are very heavy,  $m_{\tilde{q}_{L,R}} \sim 2$  TeV, precise mass reconstruction will be difficult.

Since the gluino is rather light in this scenario, several gluino decay channels can be exploited. The largest branching ratio for the gluino decay in our scenario is a three-body decay into neutralinos,  $BR(\tilde{g} \rightarrow \tilde{\chi}_2^0 b\bar{b}) \sim 14\%$ , followed by a subsequent three-body leptonic neutralino decay  $BR(\tilde{\chi}_2^0 \rightarrow \tilde{\chi}_1^0 \ell^+ \ell^-)$ ,  $\ell = e, \mu$  of about 6%, see Table 2. In this channel the dilepton edge will be clearly visible, since this process has low backgrounds [2]. The mass difference between the two light neutralino masses can be measured from the dilepton edge with an uncertainty of about [11]:

$$\delta(m_{\tilde{\chi}_2^0} - m_{\tilde{\chi}_1^0}) \sim 0.5 \text{ GeV}. \quad (5)$$

The gluino mass can be reconstructed in a manner similar to the one proposed in [12], where the SPS1a scenario is analysed. Although our scenario is different, in both we are systematics limited due to hadronic energy scale and a similar relative uncertainty of  $\sim 2\%$  can be expected.

## 2.2 Expectations at the ILC

At the first stage of the ILC,  $\sqrt{s} \leq 500$  GeV, only light charginos and neutralinos are kinematically accessible. However, in this scenario the neutralino sector is characterized by very low production cross sections, below 1 fb, so that it might not be fully exploitable. The low cross sections are due to the mixing character of the neutralinos, see [10].

Only the chargino pair production process has high rates. We constrain our analysis to the first stage of the

ILC with  $\sqrt{s} \leq 500$  GeV and study only the  $\tilde{\chi}_1^+ \tilde{\chi}_1^-$  production.

The chargino mass can be measured at  $\sqrt{s} = 350$  and 500 GeV in the continuum, with an error of about 0.5 GeV [13,14]. This can serve to optimize the ILC scan at the threshold which, because of the steepness of the  $s$ -wave excitation curve in  $\tilde{\chi}_1^+ \tilde{\chi}_1^-$  production, can be used to determine the light chargino mass very precisely, to about [14]:

$$m_{\tilde{\chi}_1^\pm} = 117.1 \pm 0.1 \text{ GeV}. \quad (6)$$

The mass of the lightest neutralino  $m_{\tilde{\chi}_1^0}$  can be derived via the decays of the light chargino, either from the energy distribution of the lepton  $\ell^-$  ( $BR(\tilde{\chi}_1^- \rightarrow \tilde{\chi}_1^0 \ell^- \bar{\nu}_\ell) \sim 11\%$ , see Table 2) or from the invariant mass distribution of the two jets in hadronic decays ( $BR(\tilde{\chi}_1^- \rightarrow \tilde{\chi}_1^0 q d \bar{q}_u) \sim 33\%$ , see Table 2). We take [14]

$$m_{\tilde{\chi}_1^0} = 59.2 \pm 0.2 \text{ GeV}. \quad (7)$$

Together with the information from the LHC, Eq. (5), a mass uncertainty for the second lightest neutralino of about

$$m_{\tilde{\chi}_2^0} = 117.1 \pm 0.5 \text{ GeV} \quad (8)$$

can be assumed.

We identify the chargino pair production process,  $e^+ e^- \rightarrow \tilde{\chi}_1^+ \tilde{\chi}_1^-$ , in the fully leptonic ( $\ell^+ \nu \tilde{\chi}_1^0 \ell^- \bar{\nu} \tilde{\chi}_1^0$ ) and semileptonic ( $\ell \nu \tilde{\chi}_1^0 q \bar{q}' \tilde{\chi}_1^0$ ) final states (where  $\ell = e, \mu$ ). We estimate an overall selection efficiency of 50%. For both final states,  $W^+ W^-$  production is expected to be the dominant SM background. For the semileptonic (slc) final state, this background can be efficiently reduced from the reconstruction of the hadronic invariant mass.

In Table 3, we list cross sections multiplied by the branching fraction  $B_{slc} = 2 \times BR(\tilde{\chi}_1^+ \rightarrow \tilde{\chi}_1^0 \bar{q} d q_u) \times BR(\tilde{\chi}_1^- \rightarrow \tilde{\chi}_1^0 \ell^- \bar{\nu}) + [BR(\tilde{\chi}_1^- \rightarrow \tilde{\chi}_1^0 \ell^- \bar{\nu})]^2 \sim 0.34$  (first two families) including an  $e_{slc} = 50\%$  selection efficiency. The error includes the statistical uncertainty based on  $\mathcal{L} = 200 \text{ fb}^{-1}$  in each polarization configuration,  $(P_{e-}, P_{e+}) = (-90\%, +60\%)$  and  $(+90\%, -60\%)$ , and a relative uncertainty in the polarization of  $\Delta P_{e\pm}/P_{e\pm} = 0.5\%$  [15].

The statistical error on the forward-backward asymmetry  $A_{FB}$ , based on binomial distribution, is given by

$$\Delta(A_{FB})^{\text{stat}} = 2\sqrt{\epsilon(1-\epsilon)/N}, \quad (9)$$

where  $\sigma_{F,B}$  are the acceptance-corrected cross sections,  $\epsilon = \sigma_F/(\sigma_F + \sigma_B)$  and  $N$  denotes the number of selected events. In Table 3 the asymmetries are listed only for the  $(P_{e-}, P_{e+}) = (-90\%, +60\%)$  case, since the cross sections for the opposite polarization are very small and the statistical errors become very large. Consequently we do not include them in the following analysis.

## 3 Parameter determination

We determine the underlying SUSY parameters in several steps:

- In the first step we use only the masses of  $\tilde{\chi}_1^\pm$ ,  $\tilde{\chi}_1^0$ ,  $\tilde{\chi}_2^0$  and the chargino pair production cross section, including the full leptonic and the semileptonic decays as observables. A four-parameter fit for the parameters  $M_1$ ,  $M_2$ ,  $\mu$  and  $m_{\tilde{\nu}}$  has been applied.
- In the second step we include as an additional observable the leptonic forward–backward asymmetry. Only the semileptonic and purely leptonic decays were used. The  $SU(2)$  relation between the two virtual masses  $m_{\tilde{\nu}}$  and  $m_{\tilde{e}_L}$  has been applied as an external constraint.
- As an attempt to test the  $SU(2)$  mass relation for the slepton and sneutrino masses, in the last step both the leptonic and hadronic forward–backward asymmetries have been used. A six-parameter fit for the parameters  $M_1$ ,  $M_2$ ,  $\mu$ ,  $m_{\tilde{\nu}}$ ,  $m_{\tilde{e}_L}$  and  $\tan\beta$  has been applied.

#### a) Analysis without forward–backward asymmetry

We use as observables the masses  $m_{\tilde{\chi}_1^\pm}$ ,  $m_{\tilde{\chi}_{1,2}^0}$  and the polarized chargino cross section multiplied by the branching ratios of semileptonic chargino decays, see Section 2.2 and Table 3.

We apply a four-parameter fit for the parameters  $M_1$ ,  $M_2$ ,  $\mu$  and  $m_{\tilde{\nu}_e}$  for fixed values of  $\tan\beta = 5, 10, 15, 20, 25, 30, 50$  and  $100$ . Fixing  $\tan\beta$  is necessary for a proper convergence of the *fitting* procedure because of the strong correlation among parameters [10]. We perform a  $\chi^2$  test. It turns out that for  $\tan\beta < 1.7$  the measurements are inconsistent with theoretical predictions at least at the  $1\sigma$  level. We obtain:

$$\begin{aligned} 59.4 &\leq M_1 \leq 62.2 \text{ GeV}, \\ 118.7 &\leq M_2 \leq 127.5 \text{ GeV}, \\ 450 &\leq \mu \leq 750 \text{ GeV}, \\ 1800 &\leq m_{\tilde{\nu}_e} \leq 2210 \text{ GeV}. \end{aligned}$$

Figure 1 shows the migration of  $1\sigma$  contours in  $m_{\tilde{\nu}_e}$ – $M_2$  (left),  $M_2$ – $\mu$  (middle) and  $M_1$ – $M_2$  (right), the other two parameters being fixed at the values determined by the minimum of  $\chi^2$  for  $\tan\beta$  changing from 5 to 10, 20 and 50.

#### b) Analysis including leptonic forward–backward asymmetry

We now extend the fit by using as additional observable the leptonic forward–backward asymmetry for polarized beams ( $-90\%$ ,  $+60\%$ ).

As a result the multiparameter fit strongly improves the results. No assumption on  $\tan\beta$  has to be made in the fit since for too small or too large values of  $\tan\beta$  the wrong value of  $A_{FB}$  is predicted. We find

$$\begin{aligned} 59.7 &\leq M_1 \leq 60.35 \text{ GeV}, \\ 119.9 &\leq M_2 \leq 122.0 \text{ GeV}, \\ 500 &\leq \mu \leq 610 \text{ GeV}, \\ 1900 &\leq m_{\tilde{\nu}_e} \leq 2100 \text{ GeV}, \\ 14 &\leq \tan\beta \leq 31. \end{aligned}$$

The constraints for the mass  $m_{\tilde{\nu}_e}$  are improved by a factor of about 2 and for gaugino mass parameters  $M_1$

and  $M_2$  by a factor of about 5, as compared to the results of previous section with unconstrained  $\tan\beta$ . The error for the higgsino mass parameter  $\mu$  also decreases significantly. Taking the constraints of eq. (10) leads to a prediction of

$$\begin{aligned} 506 &< m_{\tilde{\chi}_3^0} < 615 \text{ GeV}, \\ 512 &< m_{\tilde{\chi}_4^0} < 619 \text{ GeV}, \\ 514 &< m_{\tilde{\chi}_2^\pm} < 621 \text{ GeV}. \end{aligned}$$

#### c) Analysis including hadronic and leptonic forward–backward asymmetries: test of $SU(2)$

With the constraints for the squark masses from the LHC, the hadronic forward–backward asymmetry could be used to control the sneutrino mass. The leptonic forward–backward asymmetry provides constraints on the selectron mass and the  $SU(2)$  relation could be tested.

We perform a scan of the parameter space, taking light chargino and neutralino masses, 4 cross section and leptonic asymmetry measurements and apply a  $\chi^2$  test. We derive the following constraints:

$$\begin{aligned} 59.30 &\leq M_1 \leq 60.80 \text{ GeV}, \\ 117.8 &\leq M_2 \leq 124.2 \text{ GeV}, \\ 420 &\leq \mu \leq 950 \text{ GeV}, \\ 1860 &\leq m_{\tilde{\nu}_e} \leq 2200 \text{ GeV}, \\ 1400 \text{ GeV} &\leq m_{\tilde{e}_L}, \\ 11 &\leq \tan\beta. \end{aligned}$$

Including hadronic forward–backward asymmetry improves the constraints as follows:

$$\begin{aligned} 59.45 &\leq M_1 \leq 60.80 \text{ GeV}, \\ 118.6 &\leq M_2 \leq 124.2 \text{ GeV}, \\ 420 &\leq \mu \leq 770 \text{ GeV}, \\ 1900 &\leq m_{\tilde{\nu}_e} \leq 2120 \text{ GeV}, \\ 1500 \text{ GeV} &\leq m_{\tilde{e}_L}, \\ 11 &\leq \tan\beta \leq 60. \end{aligned}$$

The most significant change is for the sneutrino mass, for which error bars become smaller by  $\sim 50\%$ . Also an upper limit on  $\tan\beta$  is found. However we do not get an upper limit for the selectron mass. Nevertheless, the results for the selectron and sneutrino masses are consistent with the  $SU(2)$  relation.

## 4 Conclusions

Scenarios with heavy scalar particles seem to be very challenging for determining the MSSM parameters since only a very limited amount of experimental information can be accessible.

A very powerful tool in this kind of analysis turns out to be the forward–backward asymmetry. This asymmetry is strongly dependent on the mass of the exchanged heavy particle. If the  $SU(2)$  constraint is applied, the slepton masses can be determined to a precision of about 5% for masses around 2 TeV at the

**Table 1.** Masses of the SUSY particles (in GeV).

$m_{\tilde{\chi}_1^\pm}$	$m_{\tilde{\chi}_2^\pm}$	$m_{\tilde{\chi}_1^0}$	$m_{\tilde{\chi}_2^0}$	$m_{\tilde{\chi}_3^0}$	$m_{\tilde{\chi}_4^0}$	$m_h$
117	552	59	117	545	550	119
$m_{H,A}$	$m_{H^\pm}$	$m_{\tilde{\nu}_e}$	$m_{\tilde{e}_R}$	$m_{\tilde{e}_L}$	$m_{\tilde{\tau}_1}$	$m_{\tilde{\tau}_2}$
1934	1935	1994	1996	1998	1930	1963
$m_{\tilde{g}}$	$m_{\tilde{q}_R}$	$m_{\tilde{q}_L}$	$m_{\tilde{t}_1}$	$m_{\tilde{t}_2}$		
416	2002	2008	1093	1584		

**Table 2.** Branching ratios for some important decay modes in the studied MSSM scenario,  $\ell = e, \mu, \tau$ ,  $q_u = u, c$ ,  $q_d = d, s$ . Numbers are given for each family separately.

Mode	$\tilde{g} \rightarrow \tilde{\chi}_2^0 b\bar{b}$	$\tilde{g} \rightarrow \tilde{\chi}_1^- q_u \bar{q}_d$	$\tilde{\chi}_1^+ \rightarrow \tilde{\chi}_1^0 \bar{q}_d q_u$
BR	14.4%	10.8%	33.5%
Mode	$\tilde{\chi}_2^0 \rightarrow \tilde{\chi}_1^0 \ell^+ \ell^-$	$\tilde{t}_{1,2} \rightarrow \tilde{g} t$	$\tilde{\chi}_1^- \rightarrow \tilde{\chi}_1^0 \ell^- \bar{\nu}_\ell$
BR	3.0%	66%	11.0%

**Table 3.** Cross sections for the process  $e^+e^- \rightarrow \tilde{\chi}_1^+ \tilde{\chi}_1^-$  and forward-backward asymmetries ( $A_{FB}$ ) in the leptonic  $\tilde{\chi}_1^- \rightarrow \tilde{\chi}_1^0 \ell^- \bar{\nu}$  and hadronic  $\tilde{\chi}_1^- \rightarrow \tilde{\chi}_1^0 s \bar{c}$  decay modes, for different beam polarization  $P_{e^-}$ ,  $P_{e^+}$  configurations at cms  $\sqrt{s} = 350$  GeV and 500 GeV at the ILC. Concerning the errors, see text.

	$(P_{e^-}, P_{e^+})$	$(P_{e^-}, P_{e^+})$
$\sqrt{s} = 350\text{GeV}$	$(-90\%, +60\%)$	$(+90\%, -60\%)$
$\sigma(\tilde{\chi}_1^+ \tilde{\chi}_1^-)/\text{fb}$	6195.5	85.0
$\sigma(\tilde{\chi}_1^+ \tilde{\chi}_1^-) B_{slc} e_{slc}/\text{fb}$	$1062.5 \pm 4.0$	$14.6 \pm 0.7$
$A_{FB}(\ell^-)/\%$	$4.42 \pm 0.29$	–
$A_{FB}(\bar{c})/\%$	$4.18 \pm 0.74$	–
$\sqrt{s} = 500\text{GeV}$	$(-90\%, +60\%)$	$(+90\%, -60\%)$
$\sigma(\tilde{\chi}_1^+ \tilde{\chi}_1^-)/\text{fb}$	3041.5	40.3
$\sigma(\tilde{\chi}_1^+ \tilde{\chi}_1^-) B_{slc} e_{slc}/\text{fb}$	$521.6 \pm 2.3$	$6.9 \pm 0.4$
$A_{FB}(\ell^-)/\%$	$4.62 \pm 0.41$	–
$A_{FB}(\bar{c})/\%$	$4.48 \pm 1.05$	–

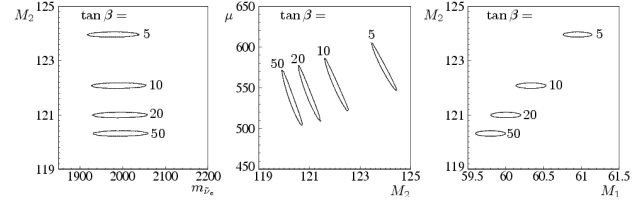
ILC running at 500 GeV. Although only very limited information is available, powerful predictions for the heavier charginos / neutralinos can be made.

### Acknowledgements

This work was supported in part by the Polish Ministry of Science and Higher Education Grant 1 P03B10830 and by the European Community's Marie-Curie Research Training Network MRTN-CT-2006-035505 (HEP-TOOLS).

### References

1. J. L. Feng, K. T. Matchev and T. Moroi, Phys. Rev. D **61** (2000) 075005 [hep-ph/9909334]; J. L. Feng and F. Wilczek, hep-ph/0507032.
2. G. Weiglein et al. [LHC/LC Study Group], Phys. Rept. 426 (2006) 47 [hep-ph/0410364].

**Fig. 1.** Migration of  $1\sigma$  contours for  $\tan\beta = 5, 10, 20, 50$  with the other two parameters fixed at the values determined by the minimum of  $\chi^2$  for each  $\tan\beta$  [10].

3. T. Tsukamoto, K. Fujii, H. Murayama, M. Yamaguchi and Y. Okada, Phys. Rev. D **51** (1995) 3153; J. L. Feng, M. E. Peskin, H. Murayama and X. Tata, Phys. Rev. D **52** (1995) 1418; H. Baer et al., hep-ph/9503479.
4. P. Bechtle, K. Desch and P. Wienemann, Comput. Phys. Commun. **174** (2006) 47 [hep-ph/0412012]; R. Lafaye, T. Plehn and D. Zerwas, hep-ph/0404282.
5. S. Y. Choi, A. Djouadi, H. K. Dreiner, J. Kalinowski and P. M. Zerwas, Eur. Phys. J. C **7** (1999) 123; S. Y. Choi, A. Djouadi, M. Guchait, J. Kalinowski, H. S. Song and P. M. Zerwas, Eur. Phys. J. C **14** (2000) 535; J. L. Kneur and G. Moultaka, Phys. Rev. D **61** (2000) 095003.
6. S. Y. Choi, J. Kalinowski, G. Moortgat-Pick and P. M. Zerwas, Eur. Phys. J. C **22** (2001) 563 [Addendum, *ibid.* C **23** (2002) 769] [hep-ph/0108117]; S. Y. Choi, J. Kalinowski, G. Moortgat-Pick and P. M. Zerwas, hep-ph/0202039. E. Boos, H. U. Martyn, G. A. Moortgat-Pick, M. Sachwitz, A. Sherstnev and P. M. Zerwas, Eur. Phys. J. C **30** (2003) 395 [hep-ph/0303110]; K. Rolbiecki, Acta Phys. Polon. B **36** (2005) 3477; S. Y. Choi, B. C. Chung, J. Kalinowski, Y. G. Kim and K. Rolbiecki, Eur. Phys. J. C **46** (2006) 511 [arXiv:hep-ph/0504122].
7. K. Desch, J. Kalinowski, G. Moortgat-Pick, M. M. Nojiri and G. Polesello, JHEP **0402** (2004) 035 [hep-ph/0312069].
8. G. Moortgat-Pick, H. Fraas, A. Bartl and W. Majerotto, Eur. Phys. J. C **7** (1999) 113 [hep-ph/9804306]; G. Moortgat-Pick and H. Fraas, Phys. Rev. D **59** (1999) 015016 [hep-ph/9708481]; G. A. Moortgat-Pick and H. Fraas, Phys. Rev. D **59** (1999) 015016 [hep-ph/9708481].
9. G. Moortgat-Pick and H. Fraas, Acta Phys. Polon. B **30** (1999) 1999 [hep-ph/9904209]; G. Moortgat-Pick, A. Bartl, H. Fraas and W. Majerotto, Eur. Phys. J. C **18** (2000) 379 [hep-ph/0007222].
10. K. Desch, J. Kalinowski, G. Moortgat-Pick, K. Rolbiecki and W. J. Stirling, JHEP **0612** (2006) 007 [hep-ph/0607104]; K. Rolbiecki, K. Desch, J. Kalinowski and G. Moortgat-Pick, hep-ph/0605168.
11. K. Kawagoe, M. M. Nojiri and G. Polesello, Phys. Rev. D **71** (2005) 035008 [hep-ph/0410160].
12. B. K. Gjelsten, D. J. Miller and P. Osland, JHEP **0506** (2005) 015 [hep-ph/0501033].
13. H. U. Martyn and G. A. Blair, hep-ph/9910416.
14. J. A. Aguilar-Saavedra et al., hep-ph/0106315; K. Abe et al., hep-ph/0109166. T. Abe et al., hep-ex/0106056.
15. G. A. Moortgat-Pick et al., hep-ph/0507011.